THE JOURNAL OF PHYSICAL CHEMISTRY C

Article

pubs.acs.org/JPCC

Characterization of V−Mo−W Mixed Oxide Catalyst Surface Species by ^{51}V Solid-State Dynamic Nuclear Polarization NMR

Aany S. L. Thankamony,[†,‡] Stefan Knoche,[§] Sarah Bothe,[†] Alfons Drochner,[§] Anil P. Jagtap,[∥] Snorri Th. Sigurdsson,[∥] Herbert Vogel,[§] Bastian J. M. Etzold,[§] Torsten Gutmann,[*,†] and Gerd Buntkowsky[*,†]

[†]Institute of Physical Chemistry, Technical University Darmstadt, Alarich-Weiss-Straße 8, D-64287 Darmstadt, Germany

[‡]Institute for Physical and Theoretical Chemistry, University Frankfurt, Max-von-Laue-Straße 7, 60438 Frankfurt, Germany

[§]Institute of Technical Chemistry, Technical University Darmstadt, Alarich-Weiss-Straße 8, D-64287 Darmstadt, Germany

[∥]Science Institute, University of Iceland, 107 Reykjavik, Iceland

Supporting Information

ABSTRACT: The investigation of V−Mo−W mixed oxide catalysts by ^{51}V DNP MAS NMR is reported. It is shown that the ^{51}V NMR signal from surface near vanadium nuclei was enhanced by a factor of ≈50 by direct polarization transfer from unpaired electrons to ^{51}V nuclei. The dependency of the DNP enhancement of the samples on different polarizing mixtures is investigated and complemented by EPR studies. V−Mo−W mixed oxide catalysts with different stoichiometry ($V_2Mo_8W_{0.5}O_y$, $V_2Mo_8W_1O_y$, and $V_2Mo_8W_{1.5}O_y$) are compared, and a suitable assignment of ^{51}V signals to different phases that are present near to the catalysts surfaces is given. Finally, the applicability of DNP solid-state NMR for the characterization of V−Mo−W mixed oxide catalysts is discussed in terms of the synthesis conditions (i.e., pH-value).

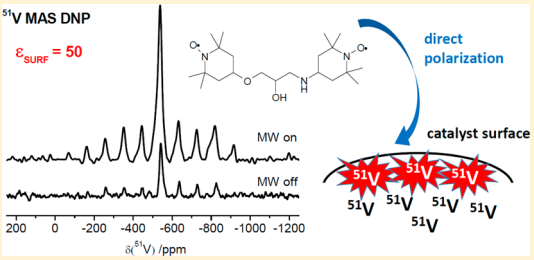

1. INTRODUCTION

Heterogeneous V−Mo−W mixed oxide catalysts are important technical catalysts used for the partial oxidation of acrolein to acrylic acid.[1−4] Acrylic acid is employed as a basic chemical for the synthesis of polymers which have widespread applications as super absorbing materials, disposable diapers, and low-phosphorus detergents. Because of their high catalytic activity and selectivity, these catalysts are used in industry for several years.[3,5]

It is known that various metal−oxygen compositions with different structures and different types of oxygen vacancies can exist on the surfaces of V−Mo−W mixed oxides, and the potential three metal redox centers Mo, V, and W, the local metal−oxygen stoichiometry and the defect structure of V−Mo-oxides play an important role in selective partial oxidation.[3] Tungsten is the crucial structural promoter in the formation and stabilization of these oxides, and vanadium is responsible for their high catalytic activity. Despite their economic importance, the nature and role of these structures are still not completely understood. Hence, in academia and industry, there is a high interest in obtaining the detailed structural information and the chemical composition of vanadium species on the surface of V−Mo−W mixed oxides. Techniques like nuclear magnetic resonance (NMR), electron paramagnetic resonance (EPR), Raman and IR spectroscopy, or the combination of these techniques with X-ray diffraction (XRD) or absorption techniques such as extended X-ray absorption fine structure (EXAFS) and X-ray absorption near edge structure spectroscopy (XANES) are suitable for such studies and were applied to characterize the structure and structural modifications of V−Mo−W mixed oxides.[6−12]

The synthesis of V−Mo−W mixed oxides with a stoichiometry of $V_2Mo_8W_xO_y$ with $0 \leq x \leq 5$ by spray drying and crystallization methods have previously been reported, as well as the characterization of the resulting catalysts by X-ray absorption spectroscopy and scanning electron microscopy (SEM).[13,14] The structural changes and phase transitions of these catalysts during the selective oxidation of acrolein to acrylic acid were studied by XRD.[15] However, the interpretation of XRD spectra of $V_2Mo_8W_xO_y$ catalysts is challenging since these catalysts contain mostly disordered structures. Moreover, XRD techniques are not able to reveal structural details, e.g., of surface sites of the material, which are, however, necessary to understand its catalytic properties.

Solid-state NMR (ssNMR) provides structural information on the local environments of NMR active nuclei, which makes it extremely useful for characterizing complex or disordered systems. As example, solid-state ^{51}V NMR spectroscopy has been used to determine the electronic structure and active sites of vanadium containing systems like metallo proteins,[16] bioinorganic solids[17−19] and inorganic catalysts.[20−23] Nowadays, the main focus of ^{51}V NMR spectroscopy is the study of

Received: July 11, 2017
Revised: August 31, 2017
Published: August 31, 2017

DOI: 10.1021/acs.jpcc.7b06761
J. Phys. Chem. C 2017, 121, 20857−20864

vanadates having catalytic properties, and of supported vanadium oxide catalysts.[24−29] Since ssNMR spectroscopy is appropriate to characterize the molecular structure and dynamics of metal oxides, its application for the analysis of the vanadium oxide phases is the focus of the present study.

Despite this tremendous application potential, ssNMR suffers from its low intrinsic sensitivity, especially when characterizing systems with low specific surface areas or low density of spins as in the case of V−Mo−W mixed oxide catalysts, for which the specific surface areas are typically in the range between 1−40 m^2/g depending on the preparation method.[14] Currently, the most efficient method to increase the sensitivity of ssNMR experiments is high field dynamic nuclear polarization (DNP) NMR combined with magic angle spinning (MAS).[30−32] With this technique, the nuclear spin polarization is enhanced by transferring polarization from unpaired electrons to nearby nuclei induced by microwave (μw) irradiation near the EPR transition frequency.

In the past few years, DNP has been successfully applied to biology and chemistry.[33−35] In parallel, the potential of high-field DNP ssNMR has been demonstrated for structure determination in materials science, for example in microcrystalline organic solids or on surfaces and subsurfaces of silicates, aluminates, nanomaterials, metal−organic frameworks (MOFs) and cellulose materials.[36−45] Recently, the first application of ^{51}V DNP NMR was demonstrated on vanadyl sulfate samples doped with TOTAPOL under MAS conditions.[46] However, to the best of our knowledge ^{51}V DNP studies of vanadium oxide catalysts or other vanadium containing technical catalysts have not yet been reported.

In the present paper, we applied high field DNP-enhanced ^{51}V MAS ssNMR spectroscopy to V−Mo−W mixed oxide technical catalysts, synthesized by a hydrothermal synthesis route. ^{51}V NMR was used to obtain information on the environment of different vanadium species and in particular to observe the vanadium ions near to the surface of the material.

The vanadium composition $V_2Mo_8W_{0.5}O_y$ (sample **1**) was investigated and compared with the data of two systems containing the same V−Mo ratios ($V_2Mo_8W_1O_y$ (sample **2**) and $V_2Mo_8W_{1.5}O_y$ (sample **3**)) but different tungsten contents (W_x). In the first step, different polarizing agents and solutions were evaluated on sample **1**, to find the optimal conditions for the DNP enhancement. These experiments were then complemented by EPR studies to support the interpretation of the observations from the DNP experiments. Finally, the efficiency of DNP in the characterization of frozen solutions of V−Mo−W mixed oxide catalysts with different tungsten contents was investigated, and the applicability of DNP for the characterization of technical V−Mo−W mixed oxide catalysts with respect to parameters of their preparation are discussed.

2. MATERIALS AND METHODS

2.1. Sample Preparation: Synthesis of V−Mo−W. The V−Mo−W mixed oxide catalysts (samples **1**−**3**) with different tungsten contents were prepared by a hydrothermal route.[47] An aqueous solution (240 mL) of ammonium heptamolybdate (Acros Organics), vanadyl sulfate hydrate (Fisher Scientific) and ammonium meta-tungstate (Sigma-Aldrich) with a desired metal ratio of the solid catalyst was taken in an autoclave. The pH-value for the preparation of sample **1** was adjusted to approximately 1.7, 2.0, 2.3, or 2.6 (sample **1** − pH x; x = 1.7, 2.0, 2.3 or 2.6), respectively, by adding dilute sulfuric acid. For the preparation of sample **2** (sample **2** − pH 2.6) and sample **3** (sample **3** − pH 2.6), only a pH-value of approximately 2.6 was employed. The reaction mixture was stirred and heated up to 448 K with 5 K min^{-1} and maintained this temperature for 24 h. After cooling, the obtained crude product was filtered, washed with water, and mixed with 120 mL of a 0.4 M oxalic acid solution. The obtained suspension was stirred for 1 h at 353−363 K. The precipitated solid was filtered, washed with water and dried overnight at 353 K. The dried precursor was calcined from room temperature to 773 K with 2 K min^{-1} under nitrogen atmosphere (N_2-flow: 100 mL min^{-1}) and maintained at 773 K for 2 h. N_2-physisorption was measured on a Quantachrome Quadrasorb at −196 °C. Prior to the measurement, the samples were degassed at 300 °C until a stable vacuum of approximately 1.3 Pa was reached. The BET specific surface area was calculated in a relative pressure range of 0.1 to 0.3.

2.2. Sample Preparation for DNP Measurements. For DNP measurements, a series of samples were prepared with different polarizing agents and solutions to compare the enhancements for sample **1** − pH 2.6 (Table 1). The polarizing agents TEKPol and AMUPol were purchased from Aix Marseille University. bTbK, TOTAPOL and bcTol were synthesized according to literature procedures.[48−50] Sample **1** − pH 2.6 was impregnated with different radical matrices namely (a) 15 mM TEKPol in ethylene tetrachloride ($EtCl_4$), (b) 15 mM bTbK in $EtCl_4$, (c) 16 mM TOTAPOL in H_2O, (d) 15 mM TOTAPOL in D_2O/H_2O (90:10) (w/w), (e) 15 mM AMUPol in D_2O/H_2O (90:10) (w/w), and (f) 10 mM bcTol in D_2O/H_2O (90:10) (w/w). An aliquot of 15 μL of the radical solution was added to cover about 30 mg of V−Mo−W mixed oxide. Sample **2** − pH 2.6 and sample **3** − pH 2.6 were impregnated with 15 mM TOTAPOL in D_2O/H_2O (90:10) (w/w), and prepared similar to sample **1** − pH 2.6, for comparison of DNP experiments.

Table 1. ^{51}V Signal Enhancements Obtained for Sample 1 − pH 2.6 Impregnated with Different Polarizing Agents and Solutions

polarizing mixture used for impregnation	absolute ^{51}V signal enhancement (ε_{ABS})	enhancement of surface ^{51}V nuclei (ε_{SURF})
15 mM TEKPol in $EtCl_4$	no detectable signal	no detectable signal
15 mM bTbK in $EtCl_4$	no Enhancement	no Enhancement
15 mM TOTAPOL in D_2O/H_2O (90:10 w/w)	5	50
16 mM TOTAPOL in H_2O	3	30
15 mM AMUPol in D_2O/H_2O	1.5	15
10 mM bcTol in D_2O/H_2O	no Enhancement	no Enhancement

2.3. DNP-Enhanced ssNMR Spectroscopy. The DNP ssNMR experiments were performed on a commercial Bruker BioSpin Avance III 400 MHz DNP NMR spectrometer equipped with a gyrotron system generating a continuous microwave (μw) of 263 GHz and a 3.2 mm triple resonance ^{1}H/X/Y low temperature MAS probe. The ^{51}V MAS NMR spectra with (MW on) and without microwave (MW off) irradiation were acquired with spinning speeds of 8 and 10 kHz and a sample temperature of nominally 110 K, which was stabilized by a Bruker BioSpin low-temperature MAS cooling system. The impregnated samples were packed into 3.2 mm sapphire rotors, sealed with a Teflon insert and a ZrO_2 drive

DOI: 10.1021/acs.jpcc.7b06761
J. Phys. Chem. C 2017, 121, 20857−20864

cap for DNP measurements. ^{51}V MAS experiments were performed at 9.4 T corresponding to a frequency of 104.5 MHz for ^{51}V. ^{51}V MAS NMR signals were recorded with a 30° excitation pulse of 1.8 μs length with a recycle delay of 1 s. The resulting spectra with (all samples) and without (only for sample **1** as a reference to determine enhancement factors) microwave irradiation were obtained from the accumulation of 30000−49000 transients corresponding to an experimental time of 8−14 h. The ^{51}V relaxation time (T_1) was measured with a saturation recovery experiment. Absolute DNP enhancement factors (ε_{ABS}) were calculated by comparing the integrals of the signals on the same sample at identical conditions with and without microwave irradiation. The typical experimental error of the calculated enhancement factors is 0.5.

The ^{51}V chemical shifts were referenced with respect to $VOCl_3$, by employing V_2O_5 (−615 ppm) as an external standard. The analysis of the ^{51}V MAS DNP spectra was performed by the deconvolution of spectra using the DMFIT software.[51] As fitting function a Lorentzian−Gaussian shape of the form $LG(x) = n*L(x) + (1 - n)*G(x)$ $(0 \leq n \leq 1)$ was used, where $L(x)$ is a Lorentzian function, $G(x)$ a Gaussian function and n the Lorentzian/Gaussian ratio. Since the line widths of the signal in each spectrum is only 120 kHz, effects of second-order quadrupolar interactions can be neglected in the interpretation of the ^{51}V spectra.

2.4. EPR Spectroscopy. The EPR spectra for all samples were measured on an EPR Miniscope MS-400 (Magnettech, Germany) equipped with a rectangular TE102 resonator operating at 9.43 GHz at room temperature. A TC H03 temperature controller was connected to the resonator for measuring and stabilizing the sample temperature. All EPR spectra were recorded with a modulation amplitude of 0.2 mT and a modulation frequency of 100 kHz. Spectra were taken under 4−20 dB of microwave attenuation with a sweep time of 30 s and 4096 data points.

3. RESULTS AND DISCUSSION

3.1. ^{51}V MAS DNP Spectra of Sample 1 − pH 2.6. Figure 1a,b shows the ^{51}V MAS NMR spectra of sample **1** − pH 2.6 impregnated with 15 mM TOTAPOL in D_2O/H_2O (90:10 w/w) recorded with (MW on) and without microwave (MW off) irradiation. The maximum signal intensity in the ^{51}V spectrum is observed at ca. −535 ppm. Comparing the intensities of the hyperpolarized signal to the intensities of the thermally polarized signal gives an absolute DNP enhancement factor $\varepsilon_{ABS} \approx 5$. In contrast to spin-1/2 X-nuclei, where spin-diffusion can be an efficient tool to transfer polarization away from the paramagnetic center, as was recently shown by Pinon et al.,[52] for quadrupolar nuclei in the presence of strong quadrupolar interactions, spin diffusion is in general very inefficient, owing to the lack of energy conserving flip-flop transitions.[53−55] For noninteger spins, a possible exception is polarization transfer between the central levels, which are in first order not affected by the quadrupolar interaction. However, such an effect would lead to a strong enhancement of the central transition compared to the satellite transitions, visible in the spinning-sidebands. As such an enhanced central transition in the DNP spectra is not observed (see Figure 1), we conclude that spin-diffusion is no efficient mechanism for the polarization transfer among the ^{51}V nuclei in our samples. Thus, it can be assumed that DNP hyperpolarizes only those nuclei, which are close to the surface of the material. From the density and specific surface area of the material, a quantitative estimation of their relative number (see Supporting Information (SI) for details) reveals that they account for ca. 10% of the overall number of ^{51}V nuclei. Thus, the enhancement factor of the surface near ^{51}V-nuclei is $\varepsilon_{SURF} \approx 50$.

This interpretation is corroborated by the differences in the line shape of the ^{51}V NMR spectra recorded with and without micro wave (Figure 2a, b). The ^{51}V signal obtained with MW on was broader by Δfwhm ≈ 2 kHz (full wide at half-maximum) compared to that with MW off. This broader ^{51}V signal in the MW on spectrum refers to ^{51}V nuclei that are near to the unpaired electrons and are experiencing large hyperfine interactions. Hence, in ^{51}V MAS DNP, the polarization of the ^{51}V nuclei close to TOTAPOL molecules is much higher than that of distant ^{51}V nuclei. Similar observations have been reported for ^{13}C and ^{29}Si direct DNP earlier.[56,57]

To investigate the influence of the polarizing mixture on the enhancement, we compared the ^{51}V DNP spectra of sample **1** − pH 2.6 with different polarizing agents and solutions. Absolute DNP enhancements of ^{51}V (ε_{ABS}) and enhancements

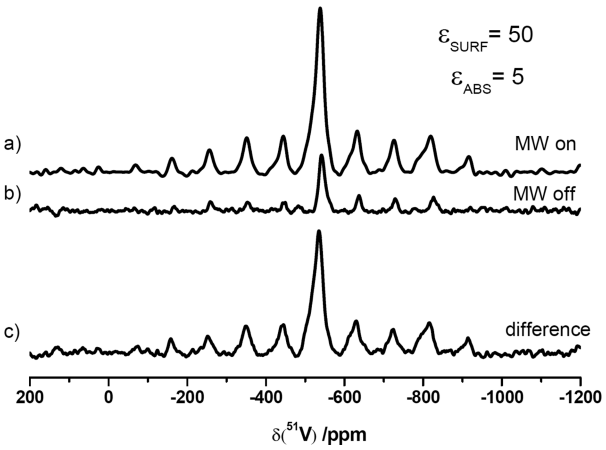

Figure 1. ^{51}V MAS DNP of $V_2Mo_8W_{0.5}O_y$ (sample **1** − pH 2.6) impregnated with 15 mM TOTAPOL in H_2O/D_2O at a spinning speed of 10 kHz, ns = 30000, recycle delay 1 s, experimental time 8 h: (a) Spectrum measured with microwave (MW on), (b) Spectrum measured without microwave (MW off) and (c) difference spectrum of spectra a and b representing only the surface near ^{51}V.

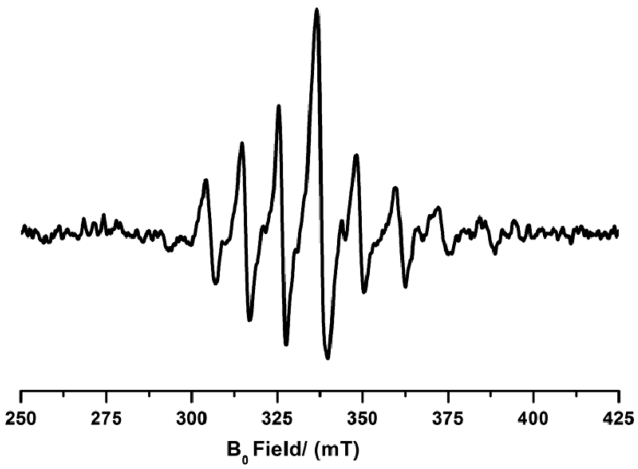

Figure 2. Continuous wave EPR spectrum of sample **1** − pH 2.6, impregnated with D_2O/H_2O (90:10 w/w) at room temperature.

DOI: 10.1021/acs.jpcc.7b06761
J. Phys. Chem. C 2017, 121, 20857−20864

of surface near ^{51}V nuclei (ε_{SURF}) for all samples are given in Table 1. No significant signal enhancement or even no signal in the ^{51}V DNP spectrum was obtained for sample **1** − pH 2.6 impregnated with 15 mM TEKPol in $EtCl_4$, 15 mM bTbK in $EtCl_4$, respectively. This is not very surprising because they are hydrophobic and the V−Mo−W mixed oxide catalyst surface is hydrophilic so that an efficient interaction between the radical and the vanadium is not feasible.

Conversely, sample **1** − pH 2.6 impregnated with 15 mM TOTAPOL in D_2O/H_2O, and with 16 mM TOTAPOL in H_2O allow good enhancement of the ^{51}V signal of sample **1** − pH 2.6. ε_{SURF} values obtained with these solutions were up to 50 and 30, respectively (Table 1). The ^{51}V spin−lattice relaxation time measured with DNP was 800 ms. Somewhat surprisingly, lower enhancement ($\varepsilon_{SURF} \approx 15$) was obtained for 15 mM AMUPol in D_2O/H_2O. For DNP ssNMR applications with AMUPol, better enhancements are expected than for TOTAPOL since the shorter DNP buildup time (T_{DNP}) for AMUPol allows faster signal averaging.[58] Thus, the lower value of 15 obtained for the AMUPol may refer to a different factor which is not fully understood and requires further investigations that are beyond the scope of paper. Most probably, paramagnetic quenching of AMUPol which is more severe than that of TOTAPOL[59] plays a relevant role. Furthermore, the fast relaxation times of vanadium and the hyperfine couplings of nearby V^{5+} nuclei with both V^{4+} and the biradical centers may lead to the loss of the signal intensity, i.e., by bleaching/quenching. This would make the enhancement lower or completely quench the signal.

3.2. EPR Results. To shed more light on our hypotheses, additional EPR measurements were performed. Figure 2 shows the EPR spectrum of sample **1** − pH 2.6 impregnated with D_2O/H_2O (90:10) solution recorded at room temperature. The spectrum consists of an octet, which is assigned to the axial hyperfine interaction between the unpaired electron spin (S = 1/2) from V^{4+} and the ^{51}V nuclear spin (I = 7/2) with a g-factor of 2.1000.[9] Such a spectral line shape[60] clearly indicates the presence of vanadyl ions (VO^{2+}) in sample **1** − pH 2.6 impregnated with D_2O/H_2O (90:10) solution. Interestingly, sample **1** − pH 2.6 in its solid form after drying the D_2O/H_2O impregnated sample, shows no EPR signals in the same region (see SI Figure S1c), which means that the aqueous solution influences the sample in a reversible way. This may be explained by the presence of water-soluble VO^{2+} species in the sample.[61−63] These VO^{2+} species dissolve into solution while impregnating the sample with the water-containing DNP matrix. Thus, the resolved EPR spectrum observed with D_2O/H_2O is mostly determined by a fast molecular tumbling of VO^{2+}, which makes the hyperfine interactions visible. To confirm this, the EPR of the filtered solution after impregnating sample **1** − pH 2.6 with D_2O/H_2O solution was measured (see SI Figure S2). The presence of an octet in the spectrum of this filtered solution supports the hypothesis that VO^{2+} present in the sample was dissolved into the solution.

Figure 3 shows the EPR spectra of sample **1** − pH 2.6 impregnated with different biradical mixtures at room temperature. The central signals at around 335 mT differ strongly from the EPR signals of the binitroxide radicals in isotropic solution, which consist of a resolved triplet splitting produced by the isotropic hyperfine coupling with the ^{14}N nucleus in these radicals.[49,58,64] This difference clearly shows that the motions of the radical moieties are restricted in sample **1** − pH 2.6 and the nitroxide radicals are interacting with sample **1** − pH 2.6.

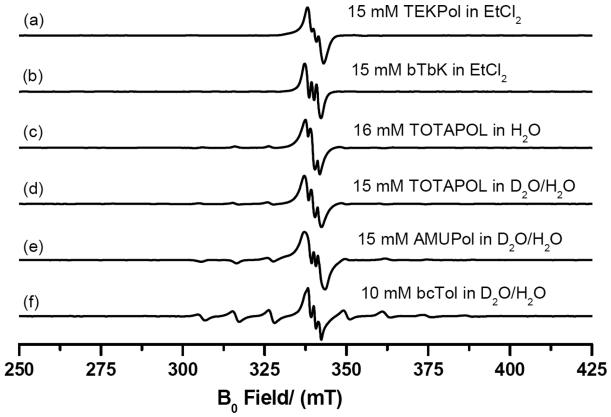

Figure 3. Continuous wave EPR spectra of sample **1** − pH 2.6 impregnated with (a) 15 mM TEKPol in $EtCl_4$, (b) 15 mM bTbK in $EtCl_4$, (c) 16 mM TOTAPOL in H_2O, (d) 15 mM TOTAPOL in D_2O/H_2O (90:10 w/w), (e) 15 mM AMUPol in D_2O/H_2O, and (f) 10 mM bcTol in D_2O/H_2O recorded at room temperature.

There are further differences between the EPR spectra of sample **1** − pH 2.6 impregnated with various polarizing matrices. The EPR spectra shown in Figure 3a,b have a similar line shape as they show only the doublet in the middle at 335 mT, which refers to the anisotropic hyperfine interaction of the biradicals. In contrary, there is a change in the EPR spectra observed for Figure 3c−f, which shows an intense doublet with additional eight less intense resonances. The doublet indeed stems from the biradicals whereas the splitting in eight resonances (two are merged by the central resonances of the biradical) results from the anisotropic hyperfine coupling of the unpaired electron spin ($S = 1/2$) from V^{+4} with the vanadium nucleus of nuclear spin $I = 7/2$.[65]

A more detailed comparison of the EPR spectrum of sample **1** − pH 2.6 in D_2O/H_2O with sample **1** − pH 2.6 in mixtures of biradicals in aqueous solution (see SI Figure S3) shows that there is a slight shift between the eight lines. This indicates that vanadium is coordinated to the biradicals, which is possible through the nitrogen or nitroxide group of the radicals.[65,66] From Figure 3c−f, the strongest intensity of the eight resonances was found for sample **1** − pH 2.6 impregnated with a 10 mM bcTol solution (Figure 3f). This strong signal intensity indicates that larger amounts of VO^{2+} are present in the bcTol system than in the case of TOTAPOL which may lead to the complete quenching of the signal. The nature of these differences in VO^{2+} concentration is not clear at the present point but is assumed to be related to the hydrophilicity of the aqueous DNP matrix which seems to be influenced by the polarity of the employed radical.

3.3. Structure Analysis by ^{51}V DNP NMR. Figure 4 shows the DNP-enhanced ^{51}V MAS spectra of $V_2Mo_8W_{0.5}O_y$ (sample **1** − pH 2.6), $V_2Mo_8W_1O_y$ (sample **2** − pH 2.6) and $V_2Mo_8W_{1.5}O_y$ (sample **3** − pH 2.6) impregnated with 15 mM TOTAPOL in D_2O/H_2O, and the deconvolution of the isotropic part of these spectra. The ^{51}V spectrum of sample **1** − pH 2.6 (Figure 4a) is dominated by an isotropic signal at ca. −535 ppm. This ^{51}V signal is asymmetric and can be deconvoluted into two lines (centered at −535 ppm and −522 ppm), which represent this line-shape in a good manner as shown in Figure 4d. Since ^{51}V reference chemical shift values of pure vanadium containing phases are not accessible, these signals were assigned with care to triclinic $(VMo)_2O_5$ and

DOI: 10.1021/acs.jpcc.7b06761
J. Phys. Chem. C 2017, 121, 20857−20864

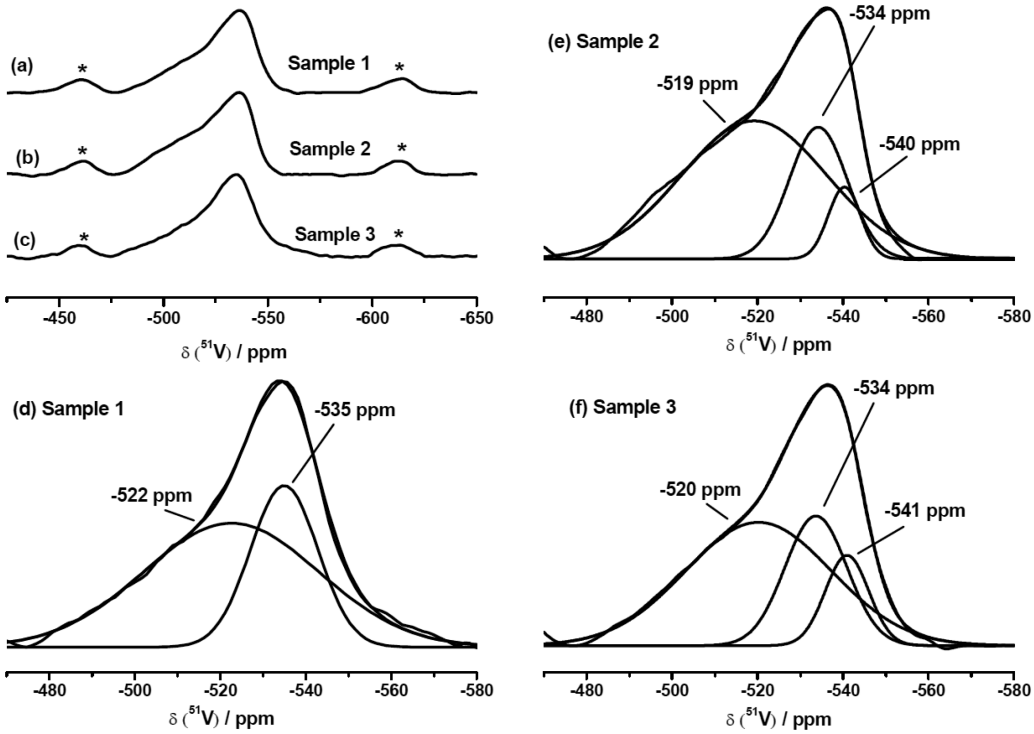

Figure 4. Comparison of the ^{51}V MAS DNP of (a) $V_2Mo_8W_{0.5}O_y$ (sample **1** − pH 2.6), (b) $V_2Mo_8W_1O_y$ (sample **2** − pH 2.6) and (c) $V_2Mo_8W_{1.5}O_y$ (sample **3** − pH 2.6) impregnated with 15 mM TOTAPOL in D_2O/H_2O. Deconvoluted ^{51}V DNP MAS NMR spectra of sample **1** − pH 2.6 (d), sample **2** − pH 2.6 (e), and sample **3** − pH 2.6 (f) impregnated with 15 mM TOTAPOL in D_2O/H_2O. Note: Measurements were performed with microwave (MW ON) at a spinning speed of 8 kHz, number of scans 45 000−49 000, according to an experimental time of ca. 14 h. Signals marked with * are spinning sidebands. The catalysts were synthesized at pH = 2.6.

hexagonal $(VMo)O_3$ phases. This assignment is based on ref 15, where it was reported that the two dominating phases of the crystallized and spray-dried $V_2Mo_8W_xO_y$ type of catalysts are hexagonal $(VMo)O_3$ and triclinic $(VMo)_2O_5$.

Figure 4b presents the DNP enhanced ^{51}V MAS spectrum of sample **2** − pH 2.6 which shows a very broad signal. The deconvolution of the signal (Figure 4e) reveals three peaks at −519, −534, and −540 ppm. The signals at −519 ppm and −534 ppm again most probably assign to hexagonal $(VMo)O_3$ and triclinic $(VMo)_2O_5$ phases while the third peak at −540 ppm seems to represent V_2MoO_8 units (according to ref 27) in which the crystal structure is closely related to octahedrally coordinated vanadium in V_2O_5.[67]

Finally, Figure 4c displays the ^{51}V DNP spectrum of sample **3** − pH 2.6, and Figure 4f is the fitted spectrum which shows three distinct vanadium peaks similar to sample **2** − pH 2.6. While the signals at −520 ppm and at −534 ppm most probably correspond to hexagonal $(VMo)O_3$ and triclinic $(VMo)_2O_5$, the third peak at −541 ppm is again attributed to V_2MoO_8 units. When comparing the spectra of the three samples, significant differences in the line-shapes were obtained which seem to be related to the tungsten content in the samples. Possibly, segregation of WO_3 that can occur with increasing tungsten content[15] influences the phase composition of the catalyst and thus cause the obtained differences.

3.4. Applicability of DNP ssNMR. To verify the reproducibility of the DNP ssNMR results, exemplarily the DNP experiments with sample **1** − pH 2.6 were repeated three times. Employing the same sample, similar signal enhancements were obtained, which demonstrates that such experiments are generally reproducible. Interestingly, when employing a sample from a different batch but with the same composition as sample **1**, the enhancements obtained from the measurements varied drastically. This led us to the assumption that the parameters employed for the preparation of the $V_2Mo_8W_xO_y$ type catalysts have a strong influence on their surface state which is detected by ssNMR combined with DNP. One very important parameter in this context is the pH value at which the catalyst is prepared. This pH value has to be adjusted with a precision of 0.1 to avoid significant differences of the catalyst structure. Here, it was found that between pH = 1.7 and pH = 2.6 a strong decrease of the concentration of V^{4+} species occurred, which is indicated by an optical color change of the washing solution of the catalysts and by preliminary EPR measurements. Furthermore, the pH-value employed for the catalyst preparation influences the obtained specific surface area. The specific surface areas of the catalysts sample **1** − pH 1.7, sample **1** − pH 2.0, sample **1** − pH 2.3 and sample **1** − pH 2.6 are 10, 41, 44, and 49 m^2/g, respectively. Consequently, the specific surface area drastically increases from 10 m^2/g to 49 m^2/g in the investigated pH range.

Both these observations are in line with results from DNP ssNMR measurements on samples prepared at slightly different pH-value (SI Figure S4). While for sample **1** − pH 1.7 no signals were obtained (SI Figure S4a), for sample **1** − pH 2.3 signals are obtained, which are enhanced (SI Figure S4b). This enhancement is even more pronounced for sample **1** − pH 2.6 (Figure 1). This observation is in agreement with the amount of V^{4+} species that seem to quench the signal enhancement due to paramagnetic relaxation. The obtained signals at high pH-value are also in line with the BET surface area which is a factor of 5 higher at pH = 2.6 compared to pH = 1.7. Thus, at pH = 2.6 a much larger quantity of surface vanadium nuclei is available that can by hyperpolarized by DNP.

DOI: 10.1021/acs.jpcc.7b06761
J. Phys. Chem. C 2017, 121, 20857−20864

4. CONCLUSION

^{51}V MAS DNP enhanced ssNMR spectroscopy is employed to investigate surface near vanadium sites in V−Mo−W mixed oxide catalysts. The optimization of the enhancement on different polarizing mixtures on $V_2Mo_8W_{0.5}O_y$ showed that the best enhancement of surface near ^{51}V nuclei with a factor of 50 is observed with TOTAPOL in D_2O/H_2O solution. The interpretation of the ^{51}V DNP enhancement for different polarization matrices is corroborated by EPR measurements, which showed that the observed enhancements strongly depend on the polarity of the solvent matrix as well as on the ability of the radical forming complexes with soluble VO^{2+}. In addition, the analysis of the ^{51}V DNP MAS NMR allowed the distinguishing of different vanadium containing phases present near the surface of the mixed oxide catalysts. Finally, the influence of the pH-value employed for the preparation of the catalyst is discussed in terms of the observed signal/signal enhancement. This analysis showed that a precise adjustment of the pH by 0.1 is necessary to produce catalysts with appropriate high surface area and low amount of V^{4+} species to enable the detection of signals/signal enhancement by ssNMR in combination with DNP.

■ ASSOCIATED CONTENT

Supporting Information

The Supporting Information is available free of charge on the ACS Publications website at DOI: 10.1021/acs.jpcc.7b06761.

Additional EPR and DNP solid-state NMR data, calculation enhancement factor (PDF)

■ AUTHOR INFORMATION

Corresponding Authors

*E-mail: gutmann@chemie.tu-darmstadt.de.
*E-mail: gerd.buntkowsky@chemie.tu-darmstadt.de.

ORCID

Snorri Th. Sigurdsson: 0000-0003-2492-1456
Torsten Gutmann: 0000-0001-6214-2272
Gerd Buntkowsky: 0000-0003-1304-9762

Notes

The authors declare no competing financial interest.

■ ACKNOWLEDGMENTS

Financial support to set up the BRUKER 400 MHz DNP NMR spectrometer by the Deutsche Forschungsgemeinschaft (DFG) under contract Bu-911-20-1 is gratefully acknowledged. The group of Prof. Vogel gratefully acknowledges financial support from the DFG contract Vo-701-10-1. The authors thank Sara Hadjiali for her technical support.

■ REFERENCES

(1) Breiter, S.; Estenfelder, M.; Lintz, H. G.; Tenten, A.; Hibst, H. The modification of the catalytic performance in the partial oxidation of acrolein by the addition of oxygen transferring compounds to a multicomponent oxidic catalyst. *Appl. Catal., A* **1996**, *134*, 81−89.

(2) Tichý, J. Oxidation of acrolein to acrylic acid over vanadium-molybdenum oxide catalysts. *Appl. Catal., A* **1997**, *157*, 363−385.

(3) Mestl, G.; Linsmeier, C.; Gottschall, R.; Dieterle, M.; Find, J.; Herein, D.; Jäger, J.; Uchida, Y.; Schlögl, R. Molybdenum oxide based partial oxidation catalyst: 1. Thermally induced oxygen deficiency, elemental and structural heterogeneity and the relation to catalytic performance. *J. Mol. Catal. A: Chem.* **2000**, *162*, 463−492.

(4) Dieterle, M.; Mestl, G.; Jäger, J.; Uchida, Y.; Hibst, H.; Schlögl, R. Mixed molybdenum oxide based partial oxidation catalyst: 2. Combined X-ray diffraction, electron microscopy and Raman investigation of the phase stability of (MoVW)5O14-type oxides. *J. Mol. Catal. A: Chem.* **2001**, *174*, 169−185.

(5) Ovsitser, O.; Uchida, Y.; Mestl, G.; Weinberg, G.; Blume, A.; Jäger, J.; Dieterle, M.; Hibst, H.; Schlögl, R. Molybdenum oxide based partial oxidation catalyst: Part 3. Structural changes of a MoVW mixed oxide catalyst during activation and relation to catalytic performance in acrolein oxidation. *J. Mol. Catal. A: Chem.* **2002**, *185*, 291−303.

(6) Erfle, S.; Armbruster, U.; Bentrup, U.; Martin, A.; Brückner, A. Impact of redox properties on dehydration of glycerol to acrolein over heteropolyacids assessed by operando-EPR spectroscopy. *Appl. Catal., A* **2011**, *391*, 102−109.

(7) Dinse, A.; Ozarowski, A.; Hess, C.; Schomäcker, R.; Dinse, K.-P. Potential of high-frequency EPR for investigation of supported vanadium oxide catalysts. *J. Phys. Chem. C* **2008**, *112*, 17664−17671.

(8) Kompio, P. G. W. A.; Brückner, A.; Hipler, F.; Auer, G.; Löffler, E.; Grünert, W. A new view on the relations between tungsten and vanadium in V2O5WO3/TiO2 catalysts for the selective reduction of NO with NH3. *J. Catal.* **2012**, *286*, 237−247.

(9) Risse, T.; Hollmann, D.; Brückner, A. In situ electron paramagnetic resonance (EPR) - a unique tool for analysing structure and reaction behaviour of paramagnetic sites in model and real catalysts. In *Catalysis*; The Royal Society of Chemistry: London, 2015; Vol. *27*, Chapter 1, pp 1−32.

(10) Uchida, Y.; Mestl, G.; Ovsitser, O.; Jäger, J.; Blume, A.; Schlögl, R. Molybdenum oxide based partial oxidation catalyst: 4. TEM identification of a new oxygen-reduced phase formed during acrolein partial oxidation under reducing conditions. *J. Mol. Catal. A: Chem.* **2002**, *187*, 247−257.

(11) Haaß, F.; Adams, A. H.; Buhrmester, T.; Schimanke, G.; Martin, M.; Fuess, H. X-Ray absorption and X-ray diffraction studies on molybdenum doped vanadium pentoxide. *Phys. Chem. Chem. Phys.* **2003**, *5*, 4317−4324.

(12) Knobl, S.; Zenkovets, G. A.; Kryukova, G. N.; Ovsitser, O.; Niemeyer, D.; Schlögl, R.; Mestl, G. The synthesis and structure of a single-phase, nanocrystalline MoVW mixed-oxide catalyst of the Mo5O14 type. *J. Catal.* **2003**, *215*, 177−187.

(13) Schimanke, G.; Martin, M.; Kunert, J.; Vogel, H. Characterization of Mo-V-W mixed oxide catalysts by ex situ and in situ X-ray absorption spectroscopy. *Z. Anorg. Allg. Chem.* **2005**, *631*, 1289−1296.

(14) Endres, S.; Kampe, P.; Kunert, J.; Drochner, A.; Vogel, H. The influence of tungsten on structure and activity of Mo−V−W-mixed oxide catalysts for acrolein oxidation. *Appl. Catal., A* **2007**, *325*, 237−243.

(15) Giebeler, L.; Kampe, P.; Wirth, A.; Adams, A. H.; Kunert, J.; Fuess, H.; Vogel, H. Structural changes of vanadium−molybdenum−tungsten mixed oxide catalysts during the selective oxidation of acrolein to acrylic acid. *J. Mol. Catal. A: Chem.* **2006**, *259*, 309−318.

(16) Fenn, A.; Wächtler, M.; Gutmann, T.; Breitzke, H.; Buchholz, A.; Lippold, I.; Plass, W.; Buntkowsky, G. Correlations between 51V solid-state NMR parameters and chemical structure of vanadium (V) complexes as models for related metalloproteins and catalysts. *Solid State Nucl. Magn. Reson.* **2009**, *36*, 192−201.

(17) Schweitzer, A.; Gutmann, T.; Wächtler, M.; Breitzke, H.; Buchholz, A.; Plass, W.; Buntkowsky, G. 51V solid-state NMR investigations and DFT studies of model compounds for vanadium haloperoxidases. *Solid State Nucl. Magn. Reson.* **2008**, *34*, 52−67.

(18) Gutmann, T.; Schweitzer, A.; Wächtler, M.; Breitzke, H.; Buchholz, A.; Plass, W.; Buntkowsky, G. DFT calculations of (51)V solid-state NMR parameters of vanadium(V) model complexes. *Z. Phys. Chem.* **2008**, *222*, 1389−1406.

(19) Wächtler, M.; Schweitzer, A.; Gutmann, T.; Breitzke, H.; Buntkowsky, G. Efficient analysis of 51V solid-state MAS NMR spectra using genetic algorithms. *Solid State Nucl. Magn. Reson.* **2009**, *35*, 37−48.

(20) Nica, S.; Buchholz, A.; Rudolph, M.; Schweitzer, A.; Wächtler, M.; Breitzke, H.; Buntkowsky, G.; Plass, W. Mixed-ligand

DOI: 10.1021/acs.jpcc.7b06761
J. Phys. Chem. C 2017, 121, 20857−20864

oxidovanadium(V) complexes with N′-salicylidenehydrazides: Synthesis, structure, and 51V solid-state MAS NMR investigation. *Eur. J. Inorg. Chem.* **2008**, *2008*, 2350−2359.
(21) Chatterjee, P. B.; Goncharov-Zapata, O.; Quinn, L. L.; Hou, G.; Hamaed, H.; Schurko, R. W.; Polenova, T.; Crans, D. C. Characterization of noninnocent metal complexes using solid-state NMR spectroscopy: o-dioxolene vanadium complexes. *Inorg. Chem.* **2011**, *50*, 9794−9803.
(22) Goncharova-Zapata, O.; Chatterjee, P. B.; Hou, G.; Quinn, L. L.; Li, M.; Yehl, J.; Crans, D. C.; Polenova, T. Effect of ancillary ligand on electronic structure as probed by 51V solid-state NMR spectroscopy for vanadium-o-dioxolene complexes. *CrystEngComm* **2013**, *15*, 8776−8783.
(23) Lapina, O. B.; Khabibulin, D. F.; Shubin, A. A.; Terskikh, V. V. Practical aspects of V-51 and Nb-93 solid-state NMR spectroscopy and applications to oxide materials. *Prog. Nucl. Magn. Reson. Spectrosc.* **2008**, *53*, 128−191.
(24) Kastner, K.; Margraf, J. T.; Clark, T.; Streb, C. A molecular placeholder strategy to access a family of transition-metal-functionalized vanadium oxide clusters. *Chem. - Eur. J.* **2014**, *20*, 12269−12273.
(25) Kunert, J.; Drochner, A.; Ott, J.; Vogel, H.; Fueß, H. Synthesis of Mo/V mixed oxide catalysts via crystallisation and spray drying a novel approach for controlled preparation of acrolein to acrylic acid catalysts. *Appl. Catal., A* **2004**, *269*, 53−61.
(26) Pourpoint, F.; Yehl, J.; Li, M.; Gupta, R.; Trébosc, J.; Lafon, O.; Amoureux, J.-P.; Polenova, T. NMR crystallography of an oxovanadium(V) complex by an approach combining multinuclear magic angle spinning NMR, DFT, and spin dynamics simulations. *ChemPhysChem* **2015**, *16*, 1619−1626.
(27) Wiench, J. W.; Fontenot, C. J.; Woodworth, J. F.; Schrader, G. L.; Pruski, M.; Larsen, S. C. Magnetic resonance investigation of vanadia and vanadium−molybdenum gels synthesized with peroxovanadate precursors. *J. Phys. Chem. B* **2005**, *109*, 1756−1762.
(28) Wachs, I. E. The generality of surface vanadium oxide phases in mixed oxide catalysts. *Appl. Catal., A* **2011**, *391*, 36−42.
(29) Eckert, H.; Wachs, I. E. Solid-state vanadium-51 NMR structural studies on supported vanadium(V) oxide catalysts: vanadium oxide surface layers on alumina and titania supports. *J. Phys. Chem.* **1989**, *93*, 6796−6805.
(30) Maly, T.; Debelouchina, G. T.; Bajaj, V. S.; Hu, K.-N.; Joo, C.-G.; Mak-Jurkauskas, M. L.; Sirigiri, J. R.; van der Wel, P. C. A.; Herzfeld, J.; Temkin, R. J.; et al. Dynamic nuclear polarization at high magnetic fields. *J. Chem. Phys.* **2008**, *128*, 052211.
(31) Afeworki, M.; McKay, R. A.; Schaefer, J. Workshop on interfaces in composite materials dynamic nuclear polarization enhanced nuclear magnetic resonance of polymer-blend interfaces. *Mater. Sci. Eng., A* **1993**, *162*, 221−228.
(32) Lelli, M.; Gajan, D.; Lesage, A.; Caporini, M. A.; Vitzthum, V.; Miéville, P.; Héroguel, F.; Rascón, F.; Roussey, A.; Thieuleux, C.; et al. Fast characterization of functionalized silica materials by silicon-29 surface-enhanced NMR spectroscopy using dynamic nuclear polarization. *J. Am. Chem. Soc.* **2011**, *133*, 2104−2107.
(33) Akbey, Ü.; Franks, W. T.; Linden, A.; Lange, S.; Griffin, R. G.; van Rossum, B.-J.; Oschkinat, H. Dynamic nuclear polarization of deuterated proteins. *Angew. Chem., Int. Ed.* **2010**, *49*, 7803−7806.
(34) Barnes, A. B.; De Paëpe, G.; van der Wel, P. C. A.; Hu, K. N.; Joo, C. G.; Bajaj, V. S.; Mak-Jurkauskas, M. L.; Sirigiri, J. R.; Herzfeld, J.; Temkin, R. J.; et al. High-field dynamic nuclear polarization for solid and solution biological NMR. *Appl. Magn. Reson.* **2008**, *34*, 237−263.
(35) Lee, D.; Duong, N. T.; Lafon, O.; De Paëpe, G. Primostrato solid-state NMR enhanced by dynamic nuclear polarization: Pentacoordinated Al3+ ions are only located at the surface of hydrated γ-alumina. *J. Phys. Chem. C* **2014**, *118*, 25065−25076.
(36) Lafon, O.; Thankamony, A. S. L.; Kobayashi, T.; Carnevale, D.; Vitzthum, V.; Slowing, I. I.; Kandel, K.; Vezin, H.; Amoureux, J.-P.; Bodenhausen, G.; et al. Mesoporous silica nanoparticles loaded with surfactant: Low temperature magic angle spinning 13C and 29Si NMR enhanced by dynamic nuclear polarization. *J. Phys. Chem. C* **2013**, *117*, 1375−1382.
(37) Gutmann, T.; Liu, J.; Rothermel, N.; Xu, Y.; Jaumann, E.; Werner, M.; Breitzke, H.; Sigurdsson, S. T.; Buntkowsky, G. Natural abundance 15N NMR by dynamic nuclear polarization: Fast analysis of binding sites of a novel amine-carboxyl-linked immobilized dirhodium catalyst. *Chem. - Eur. J.* **2015**, *21*, 3798−3805.
(38) Zhao, L.; Li, W.; Plog, A.; Xu, Y.; Buntkowsky, G.; Gutmann, T.; Zhang, K. Multi-responsive cellulose nanocrystal-rhodamine conjugates: an advanced structure study by solid-state dynamic nuclear polarization (DNP) NMR. *Phys. Chem. Chem. Phys.* **2014**, *16*, 26322−26329.
(39) Lilly Thankamony, A. S.; Lion, C.; Pourpoint, F.; Singh, B.; Perez Linde, A. J.; Carnevale, D.; Bodenhausen, G.; Vezin, H.; Lafon, O.; Polshettiwar, V. Insights into the catalytic activity of nitridated fibrous silica (KCC-1) nanocatalysts from 15N and 29Si NMR spectroscopy enhanced by dynamic nuclear polarization. *Angew. Chem., Int. Ed.* **2015**, *54*, 2190−2193.
(40) Pourpoint, F.; Thankamony, A. S. L.; Volkringer, C.; Loiseau, T.; Trebosc, J.; Aussenac, F.; Carnevale, D.; Bodenhausen, G.; Vezin, H.; Lafon, O.; et al. Probing 27Al-13C proximities in metal-organic frameworks using dynamic nuclear polarization enhanced NMR spectroscopy. *Chem. Commun.* **2014**, *50*, 933−935.
(41) Presti, C.; Thankamony, A. S. L.; Alauzun, J. G.; Mutin, P. H.; Carnevale, D.; Lion, C.; Vezin, H.; Laurencin, D.; Lafon, O. NMR and EPR characterization of functionalized nanodiamonds. *J. Phys. Chem. C* **2015**, *119*, 12408−12422.
(42) Lafon, O.; Thankamony, A. S. L.; Rosay, M.; Aussenac, F.; Lu, X.; Trebosc, J.; Bout-Roumazeilles, V.; Vezin, H.; Amoureux, J.-P. Indirect and direct 29Si dynamic nuclear polarization of dispersed nanoparticles. *Chem. Commun.* **2013**, *49*, 2864−2866.
(43) Kobayashi, T.; Perras, F. A.; Goh, T. W.; Metz, T. L.; Huang, W. Y.; Pruski, M. DNP-enhanced ultrawideline solid-state NMR spectroscopy: Studies of platinum in metal-organic frameworks. *J. Phys. Chem. Lett.* **2016**, *7*, 2322−2327.
(44) Pump, E.; Viger-Gravel, J.; Abou-Hamad, E.; Samantaray, M. K.; Hamzaoui, B.; Gurinov, A.; Anjum, D. H.; Gajan, D.; Lesage, A.; Bendjeriou-Sedjerari, A.; et al. Reactive surface organometallic complexes observed using dynamic nuclear polarization surface enhanced NMR spectroscopy. *Chem. Sci.* **2017**, *8*, 284−290.
(45) Gutmann, T.; Kumari, B.; Zhao, L.; Breitzke, H.; Schöttner, S.; Rüttiger, C.; Gallei, M. Dynamic nuclear polarization signal amplification as a sensitive probe for specific functionalization of complex paper substrates. *J. Phys. Chem. C* **2017**, *121*, 3896−3903.
(46) Perez Linde, A. J.; Carnevale, D.; Miéville, P.; Sienkiewicz, A.; Bodenhausen, G. Dynamic nuclear polarization enhancement of protons and vanadium-51 in the presence of pH-dependent vanadyl radicals. *Magn. Reson. Chem.* **2015**, *53*, 88−92.
(47) Welker-Nieuwoudt, C. A.; Karpov, A.; Rosowski, F.; Mueller-Engel, K. J.; Vogel, H.; Drochner, A.; Blickhan, N.; Duerr, N.; Jekewitz, T.; Menning, N.; Petzold, T.; Schmidt, S. Process for heterogeneously catalyzed gas phase partial oxidation of (meth)acrolein to (meth)-acrylic acid. U.S. Patent US 9181169 B2, November 10, 2015, 2014.
(48) Matsuki, Y.; Maly, T.; Ouari, O.; Karoui, H.; Le Moigne, F.; Rizzato, E.; Lyubenova, S.; Herzfeld, J.; Prisner, T.; Tordo, P.; et al. Dynamic nuclear polarization using a rigid biradical. *Angew. Chem., Int. Ed.* **2009**, *48*, 4996−5000.
(49) Song, C.; Hu, K.-N.; Joo, C.-G.; Swager, T. M.; Griffin, R. G. TOTAPOL: A biradical polarizing agent for dynamic nuclear polarization experiments in aqueous media. *J. Am. Chem. Soc.* **2006**, *128*, 11385−11390.
(50) Jagtap, A. P.; Geiger, M. A.; Stoppler, D.; Orwick-Rydmark, M.; Oschkinat, H.; Sigurdsson, S. T. bcTol: a highly water-soluble biradical for efficient dynamic nuclear polarization of biomolecules. *Chem. Commun.* **2016**, *52*, 7020−7023.
(51) Massiot, D.; Fayon, F.; Capron, M.; King, I.; Le Calvé, S.; Alonso, B.; Durand, J. O.; Bujoli, B.; Gan, Z.; Hoatson, G. Modelling one-and two-dimensional solid-state NMR spectra. *Magn. Reson. Chem.* **2002**, *40*, 70−76.
(52) Pinon, A. C.; Schlagnitweit, J.; Berruyer, P.; Rossini, A. J.; Lelli, M.; Socie, E.; Tang, M.; Pham, T.; Lesage, A.; Schantz, S.; et al.

DOI: 10.1021/acs.jpcc.7b06761
J. Phys. Chem. C 2017, 121, 20857−20864

Measuring nano- to microstructures from relayed dynamic nuclear polarization NMR. *J. Phys. Chem. C* **2017**, *121*, 15993−16005.
(53) Khutsishvili, G. Spin diffusion. *Soviet Physics Uspekhi* **1966**, *8*, 743.
(54) Eckman, R.; Pines, A.; Tycko, R.; Weitekamp, D.-P. Spin diffusion between inequivalent quadrupolar nuclei by double-quantum flip-flops. *Chem. Phys. Lett.* **1983**, *99*, 35−40.
(55) Suter, D.; Ernst, R. R. Spin diffusion in resolved solid-state NMR spectra. *Phys. Rev. B: Condens. Matter Mater. Phys.* **1985**, *32*, 5608−5627.
(56) Wind, R. A.; Duijvestijn, M. J.; van der Lugt, C.; Manenschijn, A.; Vriend, J. Applications of dynamic nuclear polarization in 13C NMR in solids. *Prog. Nucl. Magn. Reson. Spectrosc.* **1985**, *17*, 33−67.
(57) Thankamony, A. S. L.; Lafon, O.; Lu, X.; Aussenac, F.; Rosay, M.; Trébosc, J.; Vezin, H.; Amoureux, J.-P. Solvent-free high-field dynamic nuclear polarization of mesoporous silica functionalized with TEMPO. *Appl. Magn. Reson.* **2012**, *43*, 237−250.
(58) Sauvée, C.; Rosay, M.; Casano, G.; Aussenac, F.; Weber, R. T.; Ouari, O.; Tordo, P. Highly efficient, water-soluble polarizing agents for dynamic nuclear polarization at high frequency. *Angew. Chem.* **2013**, *125*, 11058−11061.
(59) Mentink-Vigier, F.; Paul, S.; Lee, D.; Feintuch, A.; Hediger, S.; Vega, S.; De Paepe, G. Nuclear depolarization and absolute sensitivity in magic-angle spinning cross effect dynamic nuclear polarization. *Phys. Chem. Chem. Phys.* **2015**, *17*, 21824−21836.
(60) Amin, S. S.; Cryer, K.; Zhang, B. Y.; Dutta, S. K.; Eaton, S. S.; Anderson, O. P.; Miller, S. M.; Reul, B. A.; Brichard, S. M.; Crans, D. C. Chemistry and insulin-mimetic properties of bis(acetylacetonate)-oxovanadium(IV) and derivatives. *Inorg. Chem.* **2000**, *39*, 406−416.
(61) Jakes, P.; Blickhan, N.; Jekewitz, T.; Drochner, A.; Vogel, H.; Fuess, H.; Eichel, R.-A. Interplay between defect structure and catalytic activity in the Mo10−xVxOy mixed-oxide system. *ChemPhysChem* **2011**, *12*, 3578−3583.
(62) Richards, R. L., Vanadium: Inorganic & Coordination Chemistry. In *Encyclopedia of Inorganic Chemistry*; John Wiley & Sons, Ltd: New York, 2006.
(63) Campbell, R. F.; Hanna, M. W. The vanadyl ion as an electron paramagnetic resonance probe of micelle-liquid crystal systems. *J. Phys. Chem.* **1976**, *80*, 1892−1898.
(64) Zagdoun, A.; Casano, G.; Ouari, O.; Schwarzwälder, M.; Rossini, A. J.; Aussenac, F.; Yulikov, M.; Jeschke, G.; Copéret, C.; Lesage, A.; et al. Large molecular weight nitroxide biradicals providing efficient dynamic nuclear polarization at temperatures up to 200 K. *J. Am. Chem. Soc.* **2013**, *135*, 12790−12797.
(65) Richardson, P. F.; Kreilick, R. W. Magnetic interactions in a vanadyl complex of an iminonitroxide radical. *Chem. Phys. Lett.* **1977**, *50*, 333−335.
(66) Richardson, P. F.; Kreilick, R. W. Complexes of free radicals with transition metals. Manganese bis(hexafluoroacetylacetonate) and vanadyl bis(trifluoroacetylacetonate) with pyridylimino nitroxide and pyridylnitronyl nitroxide radicals. *J. Phys. Chem.* **1978**, *82*, 1149−1151.
(67) Eick, H. A.; Kihlborg, L.; et al. The crystal structure of V2MoO8. *Acta Chem. Scand.* **1966**, *20*, 1658−1666.

DOI: 10.1021/acs.jpcc.7b06761
J. Phys. Chem. C 2017, 121, 20857−20864